AIP | The Journal of Chemical Physics

Rovibronic structure in slow photoelectron velocity-map imaging spectroscopy of CH2CN and CD2CN

Marissa L. Weichman, Jongjin B. Kim, and Daniel M. Neumark

Citation: The Journal of Chemical Physics **140**, 104305 (2014); doi: 10.1063/1.4867501
View online: http://dx.doi.org/10.1063/1.4867501
View Table of Contents: http://scitation.aip.org/content/aip/journal/jcp/140/10?ver=pdfcov
Published by the AIP Publishing

Rovibronic structure in slow photoelectron velocity-map imaging spectroscopy of CH_2CN^- and CD_2CN^-

Marissa L. Weichman,[1] Jongjin B. Kim,[1] and Daniel M. Neumark[1,2,a)]
[1]*Department of Chemistry, University of California, Berkeley, California 94720, USA*
[2]*Chemical Sciences Division, Lawrence Berkeley National Laboratory, Berkeley, California 94720, USA*

(Received 15 January 2014; accepted 21 February 2014; published online 12 March 2014)

We report high-resolution anion photoelectron spectra of the cryogenically cooled cyanomethide anion, CH_2CN^-, and its isotopologue, CD_2CN^-, using slow photoelectron velocity-map imaging (SEVI) spectroscopy. Electron affinities of 12 468(2) cm^{-1} for CH_2CN and 12 402(2) cm^{-1} for CD_2CN are obtained, demonstrating greater precision than previous experiments. New vibrational structure is resolved for both neutral species, especially activity of the ν_5 hydrogen umbrella modes. The ν_6 out-of-plane bending mode fundamental frequency is measured for the first time in both systems and found to be 420(10) cm^{-1} for CH_2CN and 389(8) cm^{-1} for CD_2CN. Some rotational structure is resolved, allowing for accurate extraction of vibrational frequencies. Temperature-dependent SEVI spectra show marked effects ascribed to controlled population of low-lying anion vibrational levels. We directly measure the inversion splitting between the first two vibrational levels of the anion ν_5 umbrella mode in both species, finding a splitting of 130(20) cm^{-1} for CH_2CN^- and 81(20) cm^{-1} for CD_2CN^-. Franck-Condon forbidden activity is observed and attributed to mode-specific vibrational autodetachment from the CH_2CN^- and CD_2CN^- dipole bound excited states. We also refine the binding energy of the anion dipole bound states to 39 and 42 cm^{-1}, respectively, for CH_2CN^- and CD_2CN^-. © *2014 AIP Publishing LLC*. [http://dx.doi.org/10.1063/1.4867501]

I. INTRODUCTION

The cyanomethyl radical, CH_2CN, is important astrochemically as an open-shell carbon-containing species.[1,2] It is also an intermediate in hydrocarbon combustion,[3] and is involved in thermal decomposition[4] and atmospheric reactions[5,6] of acetonitrile. The CH_2CN^- anion has been a benchmark system for ion thermochemistry studies,[7,8] and the transition from its electronic ground state to its excited dipole bound state is a plausible candidate for the 803.79 nm diffuse interstellar band (DIB).[9,10] Ground state CH_2CN^- has yet to be detected in space, though electronically analogous species like ketenimine (CH_2CNH)[11] and propadienylidene (CH_2CC)[12] have been found in the interstellar medium. Correlating astronomical microwave or IR detection of CH_2CN^- with the 803.79 nm DIB would make the case much more compelling.[13] Accurate spectroscopic characterization of CH_2CN and CH_2CN^- is crucial to their identification in astrochemical data. In the current work, we report newly resolved rovibronic structure of CH_2CN, CD_2CN, and the corresponding anions via slow photoelectron velocity-map imaging.

The cyanomethyl radical has a planar C_{2v} geometry (Fig. 1) and a $^2B_1$ ground electronic state.[14–16] The earliest studies of CH_2CN were electron spin resonance experiments carried out in a cold matrix.[17–19] In 1979, Jacox assigned IR absorption bands to the CH_2CN radical in an argon matrix.[20] The microwave spectrum of CH_2CN was observed in the laboratory in 1988 by Saito *et al.*,[14] which led to its identification in interstellar dust clouds.[1,21] More recently, it has been observed in the circumstellar shell of a carbon-rich star.[2] CH_2CN has been further characterized with high-resolution laboratory microwave spectroscopy,[15,22] and argon matrix IR absorption measurements have been made for both CH_2CN and CD_2CN.[23] The rotational structure of the ν_5 hydrogen umbrella mode of CH_2CN was studied in high resolution with IR diode laser spectroscopy.[24] Several theoretical studies have also been carried out to model the radical geometry and vibrational structure.[16,25–28]

Zimmerman and Brauman[29] found the electron affinity of CH_2CN via measurement of the total photodetachment cross-section of CH_2CN^- in 1977. The CH_2CN^- anion is closed-shell, and has a slightly non-planar C_s geometry with $^1A'$ electronic symmetry.[10,13,16,27,28,30,31] The potential along the anion ν_5 umbrella coordinate is a shallow double well. *Ab initio* calculations by Gutsev and Adamowicz[27] predict a barrier of ~150 cm^{-1} while Moran *et al.*[16] fit experimental data to yield a barrier height of 100 cm^{-1}. As the barrier is small, the anion geometry can be considered quasi-planar.[27,32,33] Schematic ν_5 bending potentials for anionic and neutral CH_2CN are illustrated in Fig. 2.

CH_2CN has a permanent dipole of at least 3.5 D,[22,27] allowing an excess electron to bind weakly to form a $^1B_1$ anionic dipole bound state (DBS).[34] The DBS has a planar C_{2v} structure like the neutral species,[10,27,32] as the dipole bound electron only weakly perturbs the molecular core. The DBSs of CH_2CN^- and CD_2CN^- have been studied with rotational autodetachment spectroscopy, first by Marks *et al.*[34] and then at considerably higher resolution by Lykke *et al.*,[32,35] who

a)Author to whom correspondence should be addressed. Electronic mail: dneumark@berkeley.edu

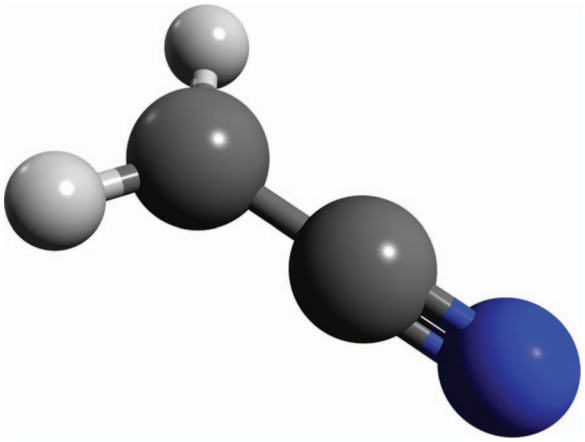

FIG. 1. Structure of the CH_2CN radical.

were able to extract rotational constants and energetics of the valence and DBS anions of both species. Lykke *et al.* placed an upper bound of 67 cm^{-1} on the binding energy of the CH_2CN^- DBS and 66 cm^{-1} on the CD_2CN^- DBS. Wetzel *et al.*[33] later studied the rotational structure of the ν_5 mode of the CH_2CN^- DBS with vibrational autodetachment spectroscopy.

Anion photoelectron spectroscopy (PES) is an attractive technique for studying neutral radicals through photodetachment of a stable closed-shell anion.[36] CH_2CN^- has been studied in several PES experiments at a resolution of $\sim$100 cm^{-1}.[16,31,37] Moran *et al.*[16] found an electron affinity of around 1.54 eV for both CH_2CN and CD_2CN, and observed that both spectra were dominated by a progression in the ν_5 umbrella mode, reflecting transitions from an anion with a small barrier to planarity to a flat neutral. In all of these experiments, the anions were at room temperature or warmer. The $\nu_5 = 1$ anion level has significant population at 300 K, leading to hot bands and congestion of the photoelectron spectra.

In the present work, we report high-resolution slow photoelectron velocity-map imaging (SEVI) spectra of the

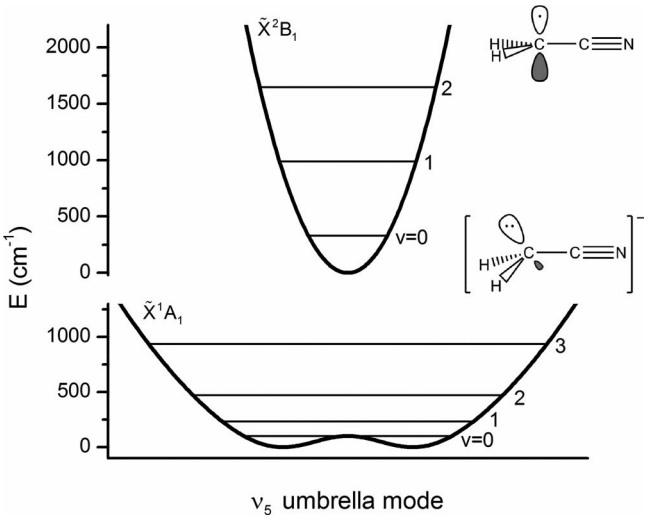

FIG. 2. Schematic of ν_5 umbrella potentials and vibrational energy levels for the anion and neutral surfaces of CH_2CN.

$\tilde{X}^2B_1 \leftarrow \tilde{X}^1A'$ transition for cryogenically cooled CH_2CN^- and CD_2CN^-. The combination of cooling with the inherent high instrumental resolution of SEVI reveals considerably more vibrational structure than was seen in previous PES studies, as well as newly resolved rotational structure. The ν_6 fundamentals of both species and the $2\nu_9$ overtone of CH_2CN are observed for the first time experimentally. The inversion splittings between the $\nu_5 = 0$ and 1 levels in both CH_2CN^- and CD_2CN^- are measured directly in temperature-dependent studies. Weak Franck-Condon (FC) forbidden modes are observed in the spectra of both isotopologues and their appearance is attributed to mode-specific autodetachment from vibrationally excited states of the anion DBSs.

II. EXPERIMENTAL METHODS

The SEVI method has been described in detail previously,[38,39] as has the current experimental setup in our laboratory.[40–42] Cryogenically cooled, mass-selected anions are photodetached with tunable light and the electron kinetic energy distribution of the resulting photoelectrons is measured with a velocity-map imaging (VMI) spectrometer. Slow electrons are preferentially detected for optimal energy resolution.

CH_2CN^- anions are prepared by expanding a dilute gas mixture of acetonitrile in He buffer gas through a pulsed Even-Lavie solenoid valve[43] fitted with a circular ionizer. CD_2CN^- anions are prepared similarly, using acetonitrile-d_3 as a precursor. Electrons from the ionizer produce slow secondary electrons that undergo dissociative attachment to acetonitrile and acetonitrile-d_3 to form the anions of interest.[44] The anions are directed to a linear octopole ion trap[40] that is cooled to as low as 5 K and filled with He/H_2 buffer gas in a 80:20 mixture. The ions are stored for $\sim$40 ms, enabling collisional cooling to their ground vibrational state before extraction into an orthogonal time-of-flight mass spectrometer.[45] After reaching the laser interaction region of the SEVI spectrometer, the mass-selected ion packet is photodetached with the output of an Nd:YAG-pumped tunable dye laser. Photoelectrons are focused with the VMI electrostatic lens[46] onto a detector consisting of two chevron-stacked micro-channel plates coupled to a phosphor screen,[47] and recorded with a CCD camera.

During data acquisition, we use event counting software to identify single electron events and compute their centroids in real time.[48] The electron kinetic energy (eKE) distribution is reconstructed from the accumulated image using the Maximum Entropy Velocity Legendre Reconstruction (MEVELER) method recently reported by Dick.[49] It is instructive to compare MEVELER to the inverse-Abel,[50] BASEX,[51] and pBASEX[52] reconstruction methods. A representative CH_2CN^- SEVI trace processed with all four methods is presented in Fig. 3. For the BASEX and pBASEX methods, the raw experimental data is Gaussian blurred with a 2 pixel standard deviation before reconstruction, so the widths of experimental features are more comparable to those of the BASEX and pBASEX basis functions. For the inverse-Abel reconstruction, each data point in the raw image is averaged

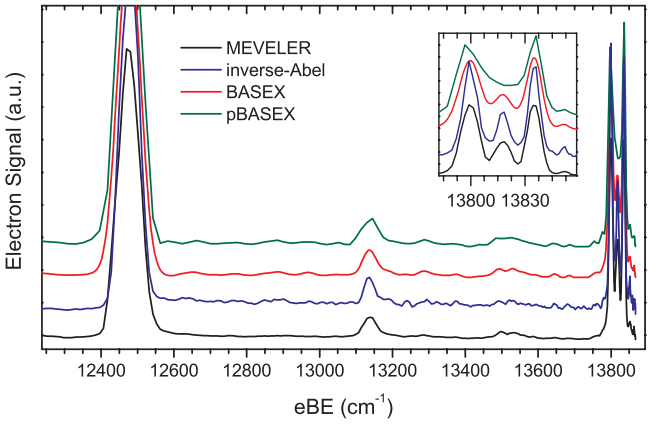

FIG. 3. Comparison of different reconstruction algorithms for one CH_2CN^- SEVI image taken at 5 K and a photon energy of 13 867 cm^{-1}. The MEVELER method (black trace), used in the current work, is compared to the inverse-Abel (blue), BASEX (red), and pBASEX (green) methods. Traces are offset vertically for clarity.

with its nearest neighbors to reduce noise in the numerical transformation.[53] The spectra processed with MEVELER are smoothed only after reconstruction and angular integration; each data point in a resulting trace is averaged with its nearest neighbors.

The spectrometer is calibrated with spectra of well-characterized photodetachment transitions[54] of atomic O^-. As the eKE depends on photodetachment laser energy ($h\nu$), we report SEVI spectra in electron binding energy (eBE), given by eBE = $h\nu$ – eKE. The VMI spectrometer has a roughly constant resolving power ΔeKE/eKE, making its resolution best for low-eKE transitions. We use small extraction voltages on the VMI electrodes to magnify the low-eKE portion of the spectrum. As described in Ref. 41, we first measure a low-resolution overview spectrum at a single photon energy. We then obtain high-resolution spectra over narrow eKE windows by measuring spectra at discrete photodetachment energies just above features of interest. These windows are merged to create a composite high-resolution spectrum of the region spanned by the overview spectrum.

III. CALCULATIONS

Electronic structure theory calculations for CH_2CN^-, CH_2CN, CD_2CN^-, and CD_2CN were carried out at the RCCSD(T)/aug-cc-pVTZ level of theory[55–57] in order to determine the geometries, normal modes, and harmonic frequencies of all species. Time-dependent density functional theory (TDDFT)[58,59] was used at the B3LYP/aug-cc-pVTZ level of theory to find the energies of excited electronic states of neutral CH_2CN. Coupled-cluster calculations were carried out using the Molpro 2010.1 software package[60] and TDDFT calculations were carried out in Q–Chem 4.0.[61,62] The geometries of the neutral species were fixed at C_{2v} symmetry in keeping with the literature,[15,16] while calculations for the anions were carried out with C_{2v} and C_s geometries. Parameters calculated for CH_2CN, CD_2CN, and their anions are summarized in Table I.

TABLE I. Energies, geometries, and harmonic frequencies for CH_2CN, CD_2CN, and their respective anions calculated at the CCSD(T)/aug–cc–pVTZ level of theory. Calculated electron affinities are given with respect to the C_s anion and are not corrected for vibrational zero-point energy. Energies are given in wavenumbers (cm^{-1}), bond lengths are given in anstroms (Å), and angles are given in degrees.

	CH_2CN^- (C_s)	CH_2CN^- (C_{2v})	CD_2CN^- (C_{2v})	CH_2CN (C_{2v})	CD_2CN (C_{2v})
EA	...	...		12 010	
$R_{H\text{-}C}$	1.087	1.082		1.080	
$R_{C\text{-}C}$	1.402	1.389		1.396	
$R_{C\text{-}N}$	1.187	1.190		1.174	
∠HCH, in-plane	115.48	119.75		120.44	
∠HCC, in-plane	116.01	120.13		119.78	
∠HCC, out-of-plane	34.77	...		...	
∠CCN, out-of-plane	176.77	...		...	
ω_1 (a_1)		3148	2283	3177	2302
ω_2 (a_1)		2087	2082	2117	2115
ω_3 (a_1)		1419	1157	1453	1155
ω_4 (a_1)		1061	922	1023	913
ω_5 (b_1)		...	...	640	527
Barrier[a]		102	102	...	...
ω_6 (b_1)		552	543	410	384
ω_7 (b_2)		3232	2407	3289	2453
ω_8 (b_2)		1015	841	1032	841
ω_9 (b_2)		418	373	361	327

[a]The barrier is calculated as the difference in energy between the optimized C_s and C_{2v} anion structures.

Rotational envelopes for the vibrational features of both isotopologues were modeled using the PGOPHER program.[63] The rotational constants for neutral CH_2CN and CD_2CN were taken from Saito *et al.*[15] while those for the corresponding anions were taken from Lykke *et al.*[32] The simulation was fit to each experimental rotational contour, with fixed rotational constants and varying band origin, temperature, and Gaussian linewidth.

IV. RESULTS

Overview SEVI spectra of the $\tilde{X}^2B_1 \leftarrow \tilde{X}^1A'$ photodetachment of CH_2CN^- and CD_2CN^- are presented in Figs. 4(a) and 4(b), respectively. Spectra of both species were taken at 5 K (black traces) and at 300 K (red traces). The temperature dependence for the low-eBE region of the spectra is examined in higher resolution in Fig. 5(a) for CH_2CN^- and Fig. 5(b) for CD_2CN^-. Both sets of spectra in Figs. 4 and 5 are highly temperature dependent. For CH_2CN^-, peaks C′ and J′, which are significant at room temperature, vanish at 5 K, while the much weaker peaks C and J become visible. The CD_2CN^- spectrum has more structure: peaks B′, C′, F′, X, Y, and Z, present at higher temperatures, are observed to vanish at 5 K, while peaks B and C become visible.

Cold, high-resolution SEVI spectra for the entire $\tilde{X}^2B_1 \leftarrow \tilde{X}^1A'$ band are shown in Figs. 6(a) and 6(b) for CH_2CN^- and CD_2CN^-, respectively. The high-resolution traces (black) are scaled to the intensity profile of the overview (blue) and are vertically offset for comparison. Both sets of spectra are dominated by intense peaks A at

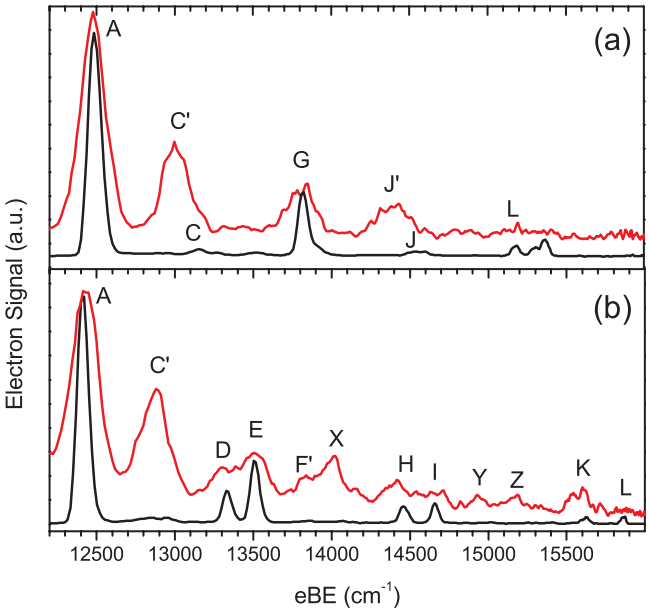

FIG. 4. Overview SEVI spectra of (a) CH_2CN^- and (b) CD_2CN^-. The black traces were taken with the ion trap held at 5 K, and with photon energies of 16 076 cm^{-1} for CH_2CN^- and 16 128 cm^{-1} for CD_2CN^-. The red traces were taken with the trap at 300 K and photon energies of 16 102 cm^{-1} for CH_2CN^- and 16 128 cm^{-1} for CD_2CN^-.

low eBE, with vibrational structure continuing for another ~3000 cm^{-1}. For both systems, no spectroscopic features are visible below the peaks labeled A, indicating that peak A represents the vibrational origin in both cases. Positions and assignments for the peaks labeled in Figs. 4–6 are summarized in Tables II and III for CH_2CN^- and CD_2CN^-. For peaks with rotational multiplet structure resolved in Fig. 6, peak positions represent the band origin found by fitting the feature's rotational contour in PGOPHER as discussed in

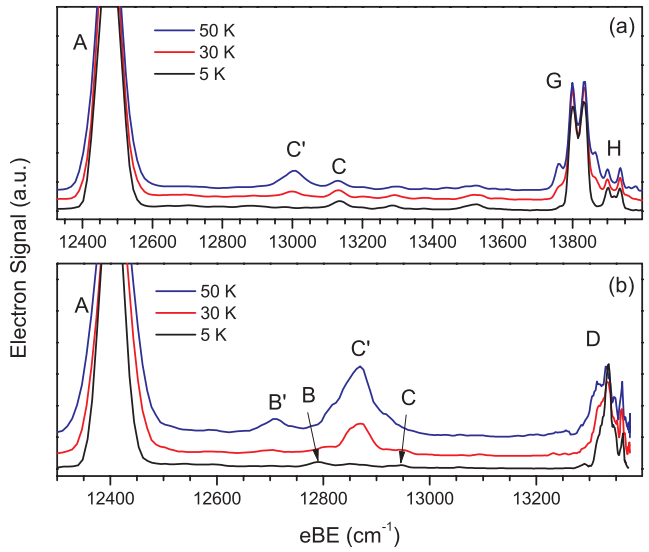

FIG. 5. Low-eBE regions of the SEVI spectra of (a) CH_2CN^- and (b) CD_2CN^- illustrating the temperature dependence of some vibrational features. The photon energy was tuned to 14 028 cm^{-1} for CH_2CN^- and to 13 376 cm^{-1} for CD_2CN^-. The ion trap temperature was set to 50 K (blue traces), 30 K (red traces), and 5 K (black traces). Traces are vertically offset for clarity.

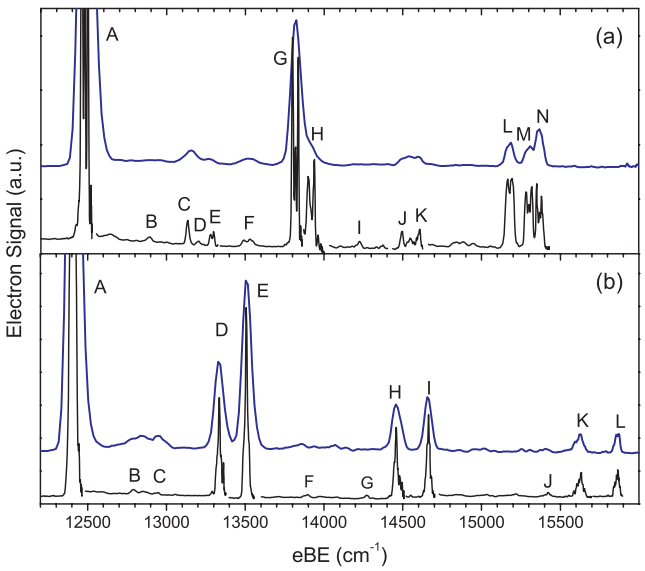

FIG. 6. SEVI spectra of (a) CH_2CN^- and (b) CD_2CN^-, taken with the ion trap held at 5 K. The blue traces are the cold low-resolution overview spectra from Fig. 4. The black traces are high-resolution composite spectra taken at many laser frequencies.

Sec. III. Positions for peaks with unresolved rotational structure (hot bands and FC forbidden features) represent the peak center found with a Gaussian fit. While SEVI's instrumental resolution is limited in this system by unusual rotational envelopes, features as narrow as 8 cm^{-1} FWHM were observed in the high-resolution spectra. Peak assignments, discussed in detail in Sec. V, were informed by the results of *ab initio* harmonic frequency calculations and values from previous studies.[16,20,23,26]

The vibrational features in the spectra of both species have distinctive rotational envelopes, discussed in more detail in Sec. V C. The vibrational origins are shown in Fig. 7,

TABLE II. Peak positions, shifts, and assignments for the SEVI spectra of CH_2CN^- given in Figs. 4(a), 5(a), and 6(a).

Peak	Position (cm^{-1})	Shift (cm^{-1})	Assignment
A	12 468	0	0_0^0
B	12 888	420	6_0^1
C′	12 997	529	5_1^1
C	13 127	659	5_0^1
D	13 200	732	9_0^2
E	13 279	811	6_0^2
F	13 495	1027	4_0^1
G	13 808	1340	5_0^2
H	13 907	1439	3_0^1
I	14 224	1756	$5_0^2 6_0^1$
J′	14 386	1918	5_1^3
J	14 483	2015	5_0^3
K	14 600	2132	$3_0^1 5_0^1$
L	15 171	2703	5_0^4
M	15 291	2823	$3_0^1 5_0^2$
N	15 360	2892	3_0^2

TABLE III. Peak positions, shifts, and assignments for the SEVI spectra of CD_2CN^- given in Figs. 4(b), 5(b), and 6(b).

Peak	Position (cm^{-1})	Shift (cm^{-1})	Assignment
A	12 402	0	0_0^0
B′	12 710	308	$5_1^0 6_0^1$
B	12 791	389	6_0^1
C′	12 865	463	5_1^1
C	12 946	544	5_0^1
D	13 331	929	$5_0^1 6_0^1$
E	13 504	1102	5_0^2
F′	13 839	1437	$5_1^2 6_0^1$
F	13 889	1487	$5_0^2 6_0^1$
X	13 998	1596	5_1^3
G	14 268	1866	$5_0^2 6_0^2$
H	14 455	2053	$5_0^3 6_0^1$
I	14 661	2259	5_0^4
Y	14 937	2535	$5_1^4 6_0^1$
Z	15 167	2765	5_1^5
J	15 420	3018	$5_0^4 6_0^2$
K	15 630	3228	$5_0^5 6_0^1$
L	15 865	3463	5_0^6

with experimental contours in black and simulations in red. In the CH_2CN^- spectrum, most vibrational modes have a characteristic three-peak rotational envelope at 5 K. The rotational contours of the CD_2CN^- spectrum have a more complex multiplet structure and are not fully resolved. The CH_2CN^- origin was fit in PGOPHER with a Gaussian linewidth of 4 cm^{-1} and an anion rotational temperature of ∼10 K, in line with previous measurements of ion temperature after extraction from our trap.[40] The CD_2CN^- contours are too poorly resolved for optimal fitting; the fit of the vibrational origin yielded a 6 cm^{-1} linewidth and an ion temperature of ∼35 K.

The relative intensities of some peaks are observed to vary dramatically as a function of photon energy. Fig. 8 shows the wavelength-dependent intensity of peak C in the SEVI spectra of both isotopologues. A dramatic increase in the relative intensity of peak C is observed with the photon energy

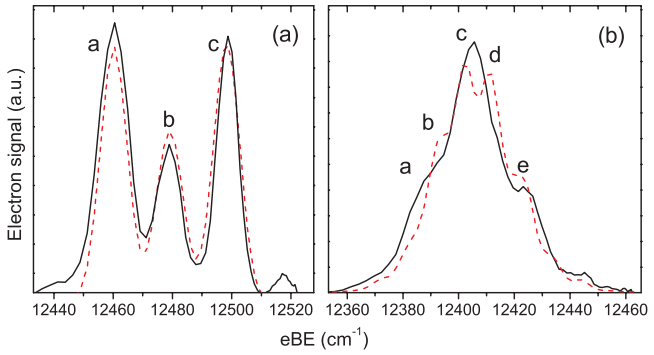

FIG. 7. Vibrational origins of the (a) CH_2CN^- and (b) CD_2CN^- high-resolution SEVI spectra, taken at 5 K and at photon energies of 12 524 cm^{-1} for CH_2CN^- and 12 463 cm^{-1} for CD_2CN^-. Experimental spectra are plotted in solid black lines, while simulated spectra are plotted in red dashed lines.

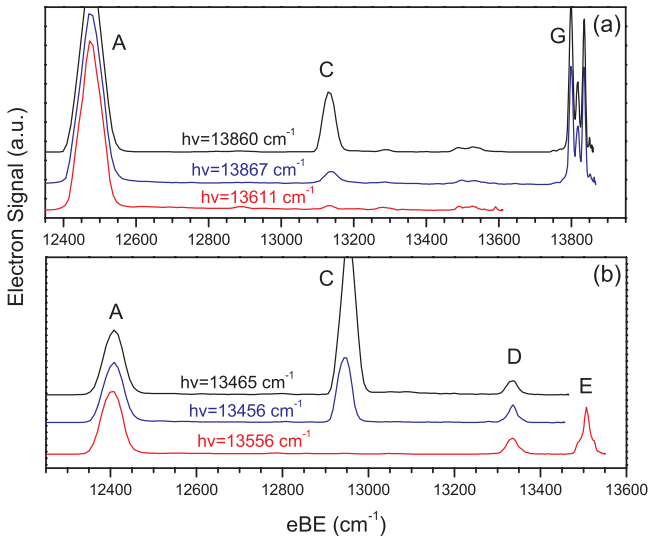

FIG. 8. SEVI spectra of (a) CH_2CN^- and (b) CD_2CN^- taken at 5 K and various photon energies, illustrating wavelength dependence of relative peak intensities.

tuned just below peak E for CD_2CN^-, and above peak G for CH_2CN^-.

Nearly all peaks in the accumulated images for both isotopologues have photoelectron angular distributions (PADs) aligned perpendicular to the laser polarization axis that shift to isotropic closer to threshold, as is expected for a $\tilde{X}^2B_1 \leftarrow \tilde{X}^1A'$ transition.[64,65] The exceptions are peaks B and C in the CH_2CN^- spectra and peak C in the CD_2CN^- spectra, which appear isotropic regardless of eKE. Peaks I, J, and K for CH_2CN^-, and peaks B and F for CD_2CN^- are too weak to accurately measure anisotropies.

V. DISCUSSION

The SEVI spectra of CH_2CN^- and CD_2CN^- demonstrate the utility of cryogenically cooling anions prior to photodetachment. With the ion trap held at 5 K, the hot bands which dominated previously reported photoelectron spectra vanish entirely.[16,31,37] This effect is demonstrated for both species in Fig. 4. In the absence of hot bands, we resolve other weak vibrational features. SEVI also provides excellent instrumental resolution (5–7 cm^{-1} in the current work) which, when combined with cooling, elucidates rotational structure and allows for more accurate extraction of vibrational frequencies through fitting of rotational contours. The spectroscopic information extracted from our experiment is summarized in Table IV, along with key results from prior work in other laboratories. Error values reported for the current work represent instrumental resolution at a given eKE, determined by one standard deviation of a Gaussian fit to a peak of atomic O^-. The exceptions are the ν_5 inversion splittings, where the reported error is one standard deviation of a Gaussian fit to the 5_1^1 hot band of each species.

The quality of the spectra were also improved by use of the MEVELER algorithm,[49] which reconstructs the eKE distribution without inversion. As demonstrated in Fig. 3, MEVELER reduces the baseline and noise of our spectra compared to the inverse-Abel method,[50] aiding interpreta-

TABLE IV. Experimental parameters from previous studies and the current work. All values are given in wavenumbers (cm^{-1}).

	CH_2CN^-	CH_2CN	CD_2CN^-	CD_2CN
Previous results				
EA		12 486(40)[a], 12 445(113)[b]		12 405(97)[b]
DBS term energy	12 428.665[c]		12 360.434[c]	
A	9.29431(14)[c]	9.506(4)[d]	4.69517(15)[c]	4.7685(1)[d]
B	0.338427(20)[c]	0.347799(2)[d]	0.300372(11)[c]	0.3029755(3)[d]
C	0.32761(21)[c]	0.329429(2)[d]	0.283102(11)[c]	0.2843613(3)[d]
ν_3		1432.3[e]		
ν_4		1026.0[e], 1028.5[f]		910.6[e]
ν_5		680[b], 664.6[e], 663.794[g], 666.4[f]		538[b], 544.4[e]
Barrier	100(50)[h]		100(50)[h]	
Inversion splitting	152[h]		101[h]	
This work				
EA		12 468(2)		12 402(2)
ν_3		1439(3)		
ν_4		1027(8)		
ν_5		659(5); $2\nu_5 = 1340(2)$		544(5); $2\nu_5 = 1105(2)$
Inversion splitting	130(20)		81(20)	
ν_6		420(10)		389(8)
ν_9		$2\nu_9 = 732(5)$		

[a]PES, Ref. 37.
[b]PES, Ref. 16.
[c]Autodetachment spectroscopy, Ref. 32.
[d]Microwave spectroscopy, Ref. 15.
[e]IR in argon matrix, Ref. 23.
[f]IR in argon matrix, Ref. 20.
[g]IR in gas phase, Ref. 24.
[h]Estimated from fitting of PES, Ref. 16.

tion. This reduction is particularly important for resolving weak features that lie between much stronger features. The spectra processed with BASEX and pBASEX are less noisy than inverse-Abel spectrum, but both introduce oscillations in the baseline that are easily mistaken for real features, and do not accurately reproduce narrow structure (see inset of Fig. 3). Baseline oscillations are much worse for BASEX[51] and pBASEX[52] if the raw images are not Gaussian blurred before reconstruction. We reach similar conclusions about the MEVELER algorithm's relative performance using simulated SEVI images, where the reconstructions can be compared to the theoretical spectrum. With simulated data, MEVELER outperforms the other reconstruction methods in reproducing peak widths and introducing the fewest baseline artifacts.

A. Vibrational assignments for CH_2CN

The CH_2CN^- SEVI spectra are dominated by the vibrational origin (peak A in Figs. 4(a), 5(a), and 6(a)) at 12 468 cm^{-1} (1.546 eV). The room-temperature spectrum (red) in Fig. 4(a) is in excellent agreement with the previously reported photoelectron spectra of CH_2CN^-.[16,31,37] At 300 K, all that is resolved is the vibrational origin (peak A), followed by a progression in the ν_5 mode (peaks C′, G, J′, and L). An intense vibrational origin indicates minimal change in geometry between anion and neutral. Extended progressions in the ν_5 umbrella mode indicate that the anion and neutral geometries differ primarily with regards to planarity.[16,31] The calculated geometries laid out in Table I support this conclusion. The optimized anion geometry is a C_s bent structure, while the planar C_{2v} structure lies on top of a barrier, calculated to be 102 cm^{-1}, along the ν_5 coordinate. As this barrier is expected to be comparable to the ν_5 vibrational zero-point energy (see Fig. 2),[16] the anion structure is effectively planar, but "floppy." The ν_5 progression in the SEVI spectrum is therefore poorly represented by a harmonic FC simulation.

The progression observed at 300 K is not regularly spaced, because transitions to neutral levels with even and odd quanta in ν_5 originate from different anion vibrational levels. The shallow double well structure of the anion ν_5 potential pushes the two lowest vibrational states closer in energy, creating a small enough gap to have a significant $\nu_5 = 1$ population at room temperature. Only transitions to neutral states with even quanta in the ν_5 mode can originate from the ground vibrational state of the anion: 5_0^2 (peak G) and 5_0^4 (peak L). Allowed transitions to neutral states with odd ν_5 quanta must originate from the anion $\nu_5 = 1$ state: 5_1^1 (peak C′) and 5_1^3(peak J′).

The hot band nature of the odd-quanta states is made clear by the 5 K spectrum shown in black in Fig. 4(a). Here, the intensities of peaks G and L are unchanged relative to A from the 300 K trace, but peaks C′ and J′ disappear entirely, as there is no significant population in the $\nu_5 = 1$ anion level at 5 K. The much weaker features C and J, visible in the absence of peaks C′ and J′, are assigned to the FC forbidden transitions 5_0^1 and 5_0^3 based on agreement with IR absorption measurements of the ν_5 fundamental in gas phase[23] and argon matrices.[20,24]

Fig. 5(a) demonstrates more clearly the temperature dependence of 5_1^1 (peak C′). The spacing between peaks C and C′ is well-resolved at temperatures of 30–50 K, giving an inversion splitting of ∼130 cm^{-1} between the $\nu_5 = 0$ and 1 levels of CH_2CN^-, close to the value of 152 cm^{-1} predicted by Moran *et al.*[16] This work is the first direct experimental determination of the splitting between these two levels.

The high-resolution composite spectrum of CH_2CN^- shown in Fig. 6(a) shows additional vibrational structure. In addition to the progression in ν_5 (peaks C, G, J, and L), we observe transitions involving the C-C-N out-of-plane bending mode 6_0^1 (peak B) and 6_0^2 (peak E), the symmetric C-C stretching mode 4_0^1 (peak F), the symmetric CH_2 scissoring mode 3_0^1 (peak H) and 3_0^2 (peak N), and, tentatively, the C-C-N in-plane bending mode 9_0^2 (peak D). We also observe combination bands $5_0^2 6_0^1$ (peak I), $3_0^1 5_0^1$ (peak K), and $3_0^1 5_0^2$ (peak M). Features involving ν_3 and ν_4 were assigned by excellent agreement with matrix IR absorption measurements by Cho and Andrews,[23] while the ν_6 and ν_9 peaks were assigned by comparison with CCSD(T)/aug-cc-pVTZ harmonic frequencies (see Table I).

Several of the observed features have b_1 vibrational symmetry (peaks B, C, I, J, and K), and are thus FC forbidden. The appearance of these peaks is ascribed to mode-specific vibrational autodetachment from the dipole bound state of CH_2CN^-, and will be discussed in detail in Sec. V D.

B. Vibrational assignments for CD_2CN

The CD_2CN SEVI spectra have an intense vibrational origin (peak A in Figs. 4(b), 5(b), and 6(b)) at 12 402 cm^{-1} (1.538 eV). While the photoelectron spectrum of CD_2CN^- taken by Moran *et al.*[16] resolved only a progression in the ν_5 mode, the SEVI overview spectra of CD_2CN^- in Fig. 4(b) reveal additional structure. The ν_5 progression (peaks C′, E, X, I, Z, and L) is accompanied by combination bands of ν_5 and the ν_6 b_1 bending mode (peaks D, F′, H, Y, and K). In the photodetachment of CH_2CN^-, analysis of our *ab initio* normal mode coordinates indicates that ν_6 primarily involves C-C-N out-of-plane bending in the anion and neutral and does not have significant Duschinsky mixing[66] with ν_5. For CD_2CN^-, calculations indicate that the ν_6 mode involves significant motion of the deuterium atoms. Duschinsky mixing of ν_5 and ν_6 between the anion and neutral normal modes therefore leads to coupled activity of ν_5 and ν_6 in the CD_2CN^- spectra.

The CD_2CN^- overview spectra exhibit numerous temperature-dependent features. In Fig. 4(b), peaks C′, F′, X, Y, and Z are present at room temperature, and vanish at 5 K, while the intensities of peaks D, E, H, I, K, and L are temperature-independent. As was true for CH_2CN^-, only transitions to neutral states with an even total number of quanta in b_1 modes are FC allowed from the ground vibrational state of the anion. Here, we assign $5_0^1 6_0^1$ (peak D), 5_0^2 (peak E), $5_0^3 6_0^1$ (peak H), 5_0^4 (peak I), $5_0^5 6_0^1$ (peak K), and 5_0^6 (peak L). The transitions to neutral states with odd quanta in b_1 modes originate from the $\nu_5 = 1$ anion state: peak C′ is assigned to 5_1^1, peak F′ to $5_1^2 6_0^1$, peak X to 5_1^3, peak Y to $5_1^4 6_0^1$, and peak Z to 5_1^5.

Fig. 5(b) gives a higher-resolution picture of the low-eBE region of the spectrum. At 5 K, two weak FC forbidden features are apparent: 6_0^1 (peak B) and 5_0^1 (peak C). At 30–50 K, two hot bands originating from the anion $\nu_5 = 1$ level are seen: peak C′, already assigned to 5_1^1, and the newly resolved peak B′, assigned to $5_1^0 6_0^1$. The gaps between peaks B and B′, and peaks C and C′ are both ∼81 cm^{-1}, yielding the inversion splitting between the first two ν_5 levels of CD_2CN^-, close to the value of 101 cm^{-1} estimated by Moran *et al.*[16]

The high-resolution SEVI spectrum of CD_2CN^- shown in Fig. 6(b) shows additional combination bands of ν_5 and ν_6: $5_0^2 6_0^1$ (peak F), $5_0^2 6_0^2$ (peak G), and $5_0^4 6_0^2$ (peak J). While these three features lie only barely above baseline noise, they are reproduced at many photon energies and are thus considered real structure. As was true for the CH_2CN^- spectra, the presence of FC forbidden vibrational features with b_1 symmetry (peaks B, C, and F) is ascribed to resonant autodetachment from the anion DBS and will be discussed in Sec. V D.

C. Rotational structure of CH_2CN and CD_2CN

Fig. 7 shows high-resolution spectra of the vibrational origins for cold CH_2CN^- and CD_2CN^- (black traces), highlighting partially-resolved rotational structure in both cases. These contours are representative of the rovibrational structure of all strong features in the spectra of each species. CH_2CN and CD_2CN are near-prolate asymmetric tops with large rotational constants around their C_2 axes: $A = 9.5$ cm^{-1} for CH_2CN and 4.8 cm^{-1} for CD_2CN.[15] Both species have two equivalent hydrogens, yielding para and ortho nuclear spin isomers. Rovibrational structure very similar to that in Fig. 7 has been observed for jet-cooled CH_2CO and CD_2CO with ZEKE and MATI photoionization techniques.[67,68] SEVI has also revealed partially resolved rotational structure in the past for the 1-propynyl radical.[69]

The selection rules that govern rovibronic transitions for the nuclear spin isomers of CH_2CN, CD_2CN, and analogous systems have been described in Refs. 32 and 68, but we summarize them here for reference. The energy levels of a slightly asymmetric prolate top can be estimated by[70]

$$E_{prolate}(J, K) = \tfrac{1}{2}(B + C)J(J + 1) + \left(A - \tfrac{1}{2}(B + C)\right)K^2, \quad (1)$$

where J and K are rotational quantum numbers, and A, B, and C are the rotational constants for the three principal axes of the molecule, with $A > B \sim C$. As B and C for both systems are much smaller than the resolution of SEVI, we cannot distinguish transitions in J, but the A values are large enough to resolve transitions in K.

The allowed values of $\Delta K = K_{neutral} - K_{anion}$ are determined by the requirement that the direct product of the total internal wavefunctions of the initial and final states be antisymmetric with respect to inversion:[71]

$$\Gamma_{rve}^{anion} \otimes \Gamma_{ns}^{anion} \otimes \Gamma_{es}^{anion} \otimes \Gamma_{rve}^{neutral} \otimes \Gamma_{ns}^{neutral} \otimes \Gamma_{es}^{neutral} \otimes \Gamma_{photoelectron} \supset \Gamma^*,$$

where Γ_{rve} is the rovibronic character of a given state, Γ_{ns} is the nuclear spin symmetry, Γ_{es} is the electron spin symmetry,

and $\Gamma_{photoelectron}$ is the electronic character of the outgoing photoelectron. The nuclear spin and electron spin will remain unchanged during the process, and $\Gamma^* = A_2$ in the C_{2v} point group, so

$$\Gamma_{rve}^{anion} \otimes \Gamma_{rve}^{neutral} \otimes \Gamma_{photoelectron} \supset A_2.$$

Assuming independent rotational, vibrational, and electronic degrees of freedom, $\Gamma_{rve} = \Gamma_{rot} \otimes \Gamma_{vib} \otimes \Gamma_{elec}$, where Γ_{elec} is a state's electronic character, Γ_{vib} is its vibrational character, and Γ_{rot} is its rotational character. For the photodetachment process under consideration, the photoelectron distributions are observed to be predominantly isotropic close to threshold and are thus attributed to s-wave ($l = 0$) electrons, so $\Gamma_{photoelectron} = A_1$. For the FC allowed peaks of both CH_2CN^- and CD_2CN^-, we are therefore left with

$$\Gamma_{rot}^{anion} \otimes \Gamma_{rot}^{neutral} \supset B_2.$$

Based on the symmetries of rotational states of C_{2v} species,[71] the allowed transitions correspond to ΔK = odd.

Nuclear spin statistics directly analogous to those of diatomic H_2 and D_2 determine the allowed rotational states for CH_2CN^- or CD_2CN^- before photodetachment. For CH_2CN^- the total internal wavefunction must be antisymmetric with respect to exchange of hydrogen atoms. Anions in ortho nuclear spin states must have odd K_{anion}, while para anions must be in rotational states with even K_{anion}.[71] The statistical ratio of ortho to para states is 3:1, so transitions originating from odd K_{anion} states of CH_2CN^- will be three times stronger than those originating from even K_{anion} states. In a SEVI experiment with anions at 5 K, we expect to see only transitions from $K_{anion} = 0$ and $K_{anion} = 1$ in a 1:3 intensity ratio.

For CD_2CN^-, the total internal wavefunction must be symmetric with respect to the exchange of deuterium atoms, yielding ortho anions with even K_{anion}, and para anions with odd K_{anion}. The statistical ratio of ortho to para states is 2:1 for CD_2CN^-. Transitions originating from $K_{anion} = 0$ states of cold CD_2CN^- will be twice as strong as those from $K_{anion} = 1$ states. Additionally, as the A constant for CD_2CN^- is small ($\sim$4.7 cm^{-1}),[32] we may see weak transitions originating from $K_{anion} = 2$ states.

The $K_{neutral} \leftarrow K_{anion}$ rotational assignments for the CH_2CN^- and CD_2CN^- vibrational origins are laid out in Table V. For CH_2CN^-, peaks a and c in Fig. 7(a) are the $0 \leftarrow 1$ and $2 \leftarrow 1$ transitions of the ortho isomer. Peak b, the $1 \leftarrow 0$ transition of the para isomer, has roughly one-third the intensity of peaks a and c, based on the nuclear spin statistics described above. These transitions are spaced by approximately $2A$, according to Eq. (1), and assuming $A_{anion} \sim A_{neutral}$ within the resolution of SEVI. Underlying the CD_2CN^- rotational envelope are the $1 \leftarrow 2$, $1 \leftarrow 0$, and $3 \leftarrow 2$ transitions of the ortho isomer (peaks a, c, and e in Fig. 7(b)), and the $0 \leftarrow 1$ and $2 \leftarrow 1$ transitions of the para isomer (peaks b and d). Peak c is roughly twice as strong as peaks b and d, in accordance with nuclear spin statistics, while peaks a and e are much weaker, originating from rotationally excited ortho states. The rotational features for CD_2CN^- are also expected to be spaced by $2A$, but are not well resolved due to the smaller rotational constant. The rotational envelopes simulated in PGOPHER (red traces in Fig. 7) reproduce the observed features, though the fit is much better for CH_2CN than for CD_2CN.

TABLE V. Rotational assignments for the SEVI spectra of the vibrational origins of CH_2CN^- and CD_2CN^- given in Figs. 7(a) and 7(b).

	Peak	Nuclear spin	Transition ($K_{neutral} \leftarrow K_{anion}$)
CH_2CN^-	a	Ortho	$0 \leftarrow 1$
	b	Para	$1 \leftarrow 0$
	c	Ortho	$2 \leftarrow 1$
CD_2CN^-	a	Ortho	$1 \leftarrow 2$
	b	Para	$0 \leftarrow 1$
	c	Ortho	$1 \leftarrow 0$
	d	Para	$2 \leftarrow 1$
	e	Ortho	$3 \leftarrow 2$

D. Vibrational autodetachment

The CH_2CN^- and CD_2CN^- SEVI spectra show FC forbidden transitions involving odd changes in vibrational quantum number in the non-totally symmetric ν_5 and ν_6 vibrational modes. The weak appearance of such features is often ascribed to Herzberg-Teller (HT) coupling through excited states of the neutral with the same overall vibronic symmetry as the forbidden feature.[42,72] Both CH_2CN and CD_2CN have a $^2B_1$ ground electronic state, so b_1 vibrational modes like ν_5 and ν_6 would have to undergo HT coupling through an A_1 neutral excited state. TDDFT calculations carried out as described in Sec. III indicate that the lowest-lying excited state with A_1 symmetry has a term energy of 5.9 eV. It is therefore unlikely for the b_1 peaks to gain intensity through HT coupling.

The strong dependence of forbidden peak intensities on photon energy suggests an alternate mechanism. Fig. 8 shows that the intensity of the 5_0^1 transition in the CH_2CN^- and CD_2CN^- spectra (peak C in both cases) is highly dependent on photon energy. When the photon energy lies just below the 5_0^2 photodetachment transition of CD_2CN^- (peak E in Fig. 8(b)), there is a dramatic spike in the relative intensity of peak C. A weaker resonance is observed for CH_2CN^- when the photon energy lies above 5_0^2 (peak G in Fig. 8(a)). In both cases, it is likely that the anion transitions to a vibrationally excited dipole bound state, and undergoes mode-specific vibrational autodetachment to the neutral $\nu_5 = 1$ state, dramatically increasing the intensity of the 5_0^1 feature in the SEVI spectrum. This mechanism is analogous to resonant autodetachment from the DBS of phenoxide recently reported by Liu *et al.*[73]

Vibrational autodetachment is a non-Born-Oppenheimer process, wherein vibrational and rotational degrees of freedom couple the autodetaching anion state to the (neutral + free electron) continuum.[74,75] The propensity rules of vibrational autodetachment parallel those of autoionization from Rydberg states.[76] Threshold autodetachment spectroscopy has been used in the past to study the CH_2CN^- and CD_2CN^- DBSs, so the electronic surfaces involved support the coupling of electronic and vibrational degrees of freedom required for vibrational autodetachment. Lykke *et al.* measured

rotational spectra of the vibrational origins of both species' DBSs with resolved J transitions,[32] while Brauman and co-workers were able to resolve K transitions in the DBS vibrational origins of both species[34] and in the 5_1^1 band of the CH_2CN^- DBS.[33] All three studies found DBS rotational structure covering extensive ranges of energy as detachment from very warm precursor ions allowed for transitions to highly excited DBS J states. As we detach from cryogenically cooled ions, we expect much sparser DBS structure. Therefore, direct detachment to the neutral is the dominant process in our experiment while autodetaching resonances occur at narrow ranges of photon energy.

Vibrational autodetachment preferentially occurs by loss of one vibrational quantum ($\Delta v = -1$) in a coupling mode whose normal coordinate changes the character of the anion orbital from which the electron is autodetached.[74,77] Brauman and co-workers[33] suggested that vibrational autodetachment from the CH_2CN^- DBS was accompanied by the loss of one quantum in ν_5. As the anion and neutral geometries differ along the ν_5 normal coordinate, displacement along ν_5 must affect the electronic character of the DBS, so it is reasonable that the ν_5 mode would couple with autodetachment.

The CH_2CN^- DBS lies 12 429 cm^{-1} above the anion ground state, and the CD_2CN^- DBS lies at 12 360 cm^{-1}.[32] By comparison to the electron affinities of CH_2CN and CD_2CN reported in this work (see Table IV), we obtain binding energies of 39 and 42 cm^{-1}, respectively, for the DBSs of CH_2CN^- and CD_2CN^-, refining the previous upper bounds of 67 and 66 cm^{-1}.[32] The vibrational frequencies of the DBSs should be quite close to those of the neutrals, as the dipole bound electron only weakly perturbs the neutral geometry.[32] The DBS vibrational levels should therefore lie ~40 cm^{-1} below their neutral counterparts in both isotopologues. This spacing is consistent with the results shown for CD_2CN^- in Fig. 8(b), where there is an enormous enhancement of 5_0^1 (peak C) when the photon energy lies ~40 cm^{-1} below 5_0^2 (peak E). Fig. 8(b) thus represents a clear instance of vibrational autodetachment from the $2\nu_5$ level of the CD_2CN^- DBS, accompanied by the loss of one quantum in ν_5. While the region just below the corresponding CH_2CN^- 5_0^2 feature (peak G in Fig. 8(a)) was not scanned for resonances, a resonance in the relative intensity of 5_0^1 (peak C) was noted with the photon energy tuned just above 5_0^2. The appearance of the other b_1 forbidden modes observed in both spectra can be ascribed to autodetachment from FC accessible DBS states by $\Delta v = -1$ processes in ν_5 or ν_6.

VI. CONCLUSIONS

We report high-resolution photoelectron spectra for the cyanomethide anion, CH_2CN^-, and its isotopologue, CD_2CN^-. With our cryogenic ion trap, we eliminate the hot bands that dominated previous photoelectron spectra of these species, allowing resolution of new vibrational features and rotational structure. We refine values for the electron affinities of CH_2CN and CD_2CN, and the binding energies of their dipole bound anions. Tunable ion trap temperature allows for control of vibrationally excited anion populations and the measurement of the inversion splitting of the lowest ν_5 levels in the ground state anions of both species. Additionally, we observe mode-specific vibrational autodetachment from the dipole bound anionic states, producing Franck-Condon forbidden features.

ACKNOWLEDGMENTS

This research is funded by the Air Force Office of Scientific Research under Grant No. FA9550-12-1-0160 and the Defense University Research Instrumentation Program under Grant No. FA9550-11-1-0300. M.L.W. thanks the National Science Foundation for a graduate research fellowship.

[1] W. M. Irvine, P. Friberg, Å. Hjalmarson, S. Ishikawa, N. Kaifu, K. Kawaguchi, S. C. Madden, H. E. Matthews, M. Ohishi, S. Saito, H. Suzuki, P. Thaddeus, B. E. Turner, S. Yamamoto, and L. M. Ziurys, Astrophys. J. **334**, L107 (1988).
[2] M. Agúndez, J. P. Fonfría, J. Cernicharo, J. R. Pardo, and M. Guélin, Astron. Astrophys. **479**, 493 (2008).
[3] K. Hoyermann and J. Seeba, Z. Phys. Chem. **188**, 215 (1995).
[4] A. Lifshitz, A. Moran, and S. Bidani, Int. J. Chem. Kinet. **19**, 61 (1987).
[5] M. J. Kurylo and G. L. Knable, J. Phys. Chem. **88**, 3305 (1984).
[6] G. Poulet, G. Laverdet, J. L. Jourdain, and G. Le Bras, J. Phys. Chem. **88**, 6259 (1984).
[7] D. A. Shea, R. J. J. M. Steenvoorden, and P. Chen, J. Phys. Chem. A **101**, 9728 (1997).
[8] R. P. Thorn, P. S. Monks, L. J. Stief, S.-C. Kuo, Z. Zhang, S. K. Ross, and R. B. Klemm, J. Phys. Chem. A **102**, 846 (1998).
[9] P. J. Sarre, Mon. Not. R. Astron. Soc. **313**, L14 (2000).
[10] M. A. Cordiner and P. J. Sarre, Astron. Astrophys. **472**, 537 (2007).
[11] F. J. Lovas, J. M. Hollis, A. J. Remijan, and P. R. Jewell, Astrophys. J. **645**, L137 (2006).
[12] J. Cernicharo, C. A. Gottlieb, M. Guélin, T. C. Killian, G. Paubert, P. Thaddeus, and J. M. Vrtilek, Astrophys. J. **368**, L39 (1991).
[13] R. C. Fortenberry, T. D. Crawford, and T. J. Lee, Astrophys. J. **762**, 121 (2013).
[14] S. Saito, S. Yamamoto, W. M. Irvine, L. M. Ziurys, H. Suzuki, M. Ohishi, and N. Kaifu, Astrophys. J. **334**, L113 (1988).
[15] S. Saito and S. Yamamoto, J. Chem. Phys. **107**, 1732 (1997).
[16] S. Moran, H. B. Ellis, D. J. DeFrees, A. D. McLean, and G. B. Ellison, J. Am. Chem. Soc. **109**, 5996 (1987).
[17] P. B. Ayscough, R. G. Collins, and T. J. Kemp, J. Phys. Chem. **70**, 2220 (1966).
[18] R. J. Egland and M. C. R. Symons, J. Chem. Soc. A **1970**, 1326.
[19] P. Svejda and D. H. Volman, J. Phys. Chem. **74**, 1872 (1970).
[20] M. E. Jacox, Chem. Phys. **43**, 157 (1979).
[21] B. E. Turner, P. Friberg, W. M. Irvine, S. Saito, and S. Yamamoto, Astrophys. J. **355**, 546 (1990).
[22] H. Ozeki, T. Hirao, S. Saito, and S. Yamamoto, Astrophys. J. **617**, 680 (2004).
[23] H.-G. Cho and L. Andrews, J. Phys. Chem. A **115**, 8638 (2011).
[24] Y. Sumiyoshi, K. Tanaka, and T. Tanaka, J. Chem. Phys. **104**, 1839 (1996).
[25] F. Delbecq, Chem. Phys. Lett. **99**, 21 (1983).
[26] M. Horn, M. Oswald, R. Oswald, and P. Botschwina, Ber. Bunsenges. Phys. Chem. **99**, 323 (1995).
[27] G. L. Gutsev and L. Adamowicz, Chem. Phys. Lett. **246**, 245 (1995).
[28] P. M. Mayer, M. S. Taylor, M. W. Wong, and L. Radom, J. Phys. Chem. A **102**, 7074 (1998).
[29] A. H. Zimmerman and J. I. Brauman, J. Am. Chem. Soc. **99**, 3565 (1977).
[30] P. G. Mezey, M. A. Robb, K. Yates, and I. G. Csizmadia, Theor. Chim. Acta **49**, 277 (1978).
[31] D. J. Goebbert, L. Velarde, D. Khuseynov, and A. Sanov, J. Phys. Chem. Lett. **1**, 792 (2010).
[32] K. R. Lykke, D. M. Neumark, T. Andersen, V. J. Trapa, and W. C. Lineberger, J. Chem. Phys. **87**, 6842 (1987).
[33] D. M. Wetzel and J. I. Brauman, J. Chem. Phys. **90**, 68 (1989).
[34] J. Marks, D. M. Wetzel, P. B. Comita, and J. I. Brauman, J. Chem. Phys. **84**, 5284 (1986).
[35] K. R. Lykke, K. K. Murray, D. M. Neumark, and W. C. Lineberger, Philos. Trans. R. Soc. London, Ser. A **324**, 179 (1988).

[36]J. C. Rienstra-Kiracofe, G. S. Tschumper, H. F. Schaefer, S. Nandi, and G. B. Ellison, Chem. Rev. **102**, 231 (2002).
[37]T. Ichino, D. H. Andrews, G. J. Rathbone, F. Misaizu, R. M. D. Calvi, S. W. Wren, S. Kato, V. M. Bierbaum, and W. C. Lineberger, J. Phys. Chem. B **112**, 545 (2008).
[38]A. Osterwalder, M. J. Nee, J. Zhou, and D. M. Neumark, J. Chem. Phys. **121**, 6317 (2004).
[39]D. M. Neumark, J. Phys. Chem. A **112**, 13287 (2008).
[40]C. Hock, J. B. Kim, M. L. Weichman, T. I. Yacovitch, and D. M. Neumark, J. Chem. Phys. **137**, 244201 (2012).
[41]J. B. Kim, M. L. Weichman, T. I. Yacovitch, C. Shih, and D. M. Neumark, J. Chem. Phys. **139**, 104301 (2013).
[42]M. L. Weichman, J. B. Kim, and D. M. Neumark, J. Chem. Phys. **139**, 144314 (2013).
[43]U. Even, J. Jortner, D. Noy, N. Lavie, and C. Cossart-Magos, J. Chem. Phys. **112**, 8068 (2000).
[44]W. Sailer, A. Pelc, P. Limão-Vieira, N. J. Mason, J. Limtrakul, P. Scheier, M. Probst, and T. D. Märk, Chem. Phys. Lett. **381**, 216 (2003).
[45]W. C. Wiley and I. H. McLaren, Rev. Sci. Instrum. **26**, 1150 (1955).
[46]A. T. J. B. Eppink and D. H. Parker, Rev. Sci. Instrum. **68**, 3477 (1997).
[47]D. W. Chandler and P. L. Houston, J. Chem. Phys. **87**, 1445 (1987).
[48]M. B. Doyle, C. Abeyasera, and A. G. Suits, NuACQ, 2012, see http://chem.wayne.edu/suitsgroup/NuACQ.html.
[49]B. Dick, Phys. Chem. Chem. Phys. **16**, 570 (2014).
[50]E. W. Hansen and P. L. Law, J. Opt. Soc. Am. A **2**, 510 (1985).
[51]V. Dribinski, A. Ossadtchi, V. A. Mandelshtam, and H. Reisler, Rev. Sci. Instrum. **73**, 2634 (2002).
[52]G. A. Garcia, L. Nahon, and I. Powis, Rev. Sci. Instrum. **75**, 4989 (2004).
[53]J. Zhou, Ph.D. thesis, University of California, Berkeley, 2007.
[54]C. Blondel, W. Chaibi, C. Delsart, C. Drag, F. Goldfarb, and S. Kröger, Eur. Phys. J. D **33**, 335 (2005).
[55]P. J. Knowles, C. Hampel, and H.-J. Werner, J. Chem. Phys. **99**, 5219 (1993).
[56]J. D. Watts, J. Gauss, and R. J. Bartlett, J. Chem. Phys. **98**, 8718 (1993).
[57]R. A. Kendall, T. H. Dunning, and R. J. Harrison, J. Chem. Phys. **96**, 6796 (1992).
[58]E. Runge and E. K. U. Gross, Phys. Rev. Lett. **52**, 997 (1984).
[59]M. E. Casida, in *Recent Advances in Density Functional Methods*, edited by D. P. Chong (World Scientific, Singapore, 1995), p. 155.
[60]H.-J. Werner, P. J. Knowles, G. Knizia, F. R. Manby, M. Schütz *et al.*, MOLPRO, version 2010.1, a package of *ab initio* programs, 2010, see http://www.molpro.net.
[61]Y. Shao, L. F. Molnar, Y. Jung, J. Kussmann, C. Ochsenfeld, S. T. Brown, A. T. B. Gilbert, L. V. Slipchenko, S. V. Levchenko, D. P. O'Neill, R. A. DiStasio, R. C. Lochan, T. Wang, G. J. O. Beran, N. A. Besley, J. M. Herbert, C. Y. Lin, T. Van Voorhis, S. H. Chien, A. Sodt, R. P. Steele, V. A. Rassolov, P. E. Maslen, P. P. Korambath, R. D. Adamson, B. Austin, J. Baker, E. F. C. Byrd, H. Dachsel, R. J. Doerksen, A. Dreuw, B. D. Dunietz, A. D. Dutoi, T. R. Furlani, S. R. Gwaltney, A. Heyden, S. Hirata, C. P. Hsu, G. Kedziora, R. Z. Khalliulin, P. Klunzinger, A. M. Lee, M. S. Lee, W. Liang, I. Lotan, N. Nair, B. Peters, E. I. Proynov, P. A. Pieniazek, Y. M. Rhee, J. Ritchie, E. Rosta, C. D. Sherrill, A. C. Simmonett, J. E. Subotnik, H. L. Woodcock, W. Zhang, A. T. Bell, A. K. Chakraborty, D. M. Chipman, F. J. Keil, A. Warshel, W. J. Hehre, H. F. Schaefer, J. Kong, A. I. Krylov, P. M. W. Gill, and M. Head-Gordon, Phys. Chem. Chem. Phys. **8**, 3172 (2006).
[62]A. I. Krylov and P. M. W. Gill, WIREs Comput. Mol. Sci. **3**, 317 (2013).
[63]C. M. Western, PGOPHER, a program for simulating rotational structure, 2010, see http://pgopher.chm.bris.ac.uk.
[64]E. Surber, R. Mabbs, and A. Sanov, J. Phys. Chem. A **107**, 8215 (2003).
[65]A. Sanov, Annu. Rev. Phys. Chem. **65**, 341 (2014).
[66]F. Duschinsky, Acta Physicochim. URSS **7**, 551 (1937).
[67]S. Willitsch, A. Haldi, and F. Merkt, Chem. Phys. Lett. **353**, 167 (2002).
[68]S. Wang, Y. Shi, Z. J. Jakubek, M. Barnett, B. Simard, K. Müller-Dethlefs, C.-P. Liu, and Y.-P. Lee, J. Chem. Phys. **117**, 6546 (2002).
[69]J. Zhou, E. Garand, W. Eisfeld, and D. M. Neumark, J. Chem. Phys. **127**, 034304 (2007).
[70]G. Herzberg, *Molecular spectra and molecular structure. Vol. 2: Infrared and Raman spectra of polyatomic molecules* (D. Van Nostrand Co., Inc., New York, 1945).
[71]P. R. Bunker and P. Jensen, *Molecular Symmetry and Spectroscopy* (NRC Research Press, Ottawa, 1998).
[72]J. B. Kim, M. L. Weichman, and D. M. Neumark, Phys. Chem. Chem. Phys. **15**, 20973 (2013).
[73]H.-T. Liu, C.-G. Ning, D.-L. Huang, P. D. Dau, and L.-S. Wang, Angew. Chem., Int. Ed. **52**, 8976 (2013).
[74]J. Simons, J. Am. Chem. Soc. **103**, 3971 (1981).
[75]T. Andersen, K. R. Lykke, D. M. Neumark, and W. C. Lineberger, J. Chem. Phys. **86**, 1858 (1987).
[76]R. S. Berry, J. Chem. Phys. **45**, 1228 (1966).
[77]J. Simons, in *Photoionization and Photodetachment*, edited by C. Y. Ng (World Scientific, Singapore, 1999), p. 958.